Published in final edited form as:

Neuron. 2019 May 22; 102(4): 887–898.e5. doi:10.1016/j.neuron.2019.03.025.

Multiplexing of Theta and Alpha Rhythms in the Amygdala-Hippocampal Circuit Supports Pattern Separation of Emotional Information

Jie Zheng[1], **Rebecca F. Stevenson**[2,3], **Bryce A. Mander**[3,4], **Lilit Mnatsakanyan**[5], **Frank P.K. Hsu**[6], **Sumeet Vadera**[6], **Robert T. Knight**[7,8], **Michael A. Yassa**[2,3,4,9,*], and **Jack J. Lin**[1,3,5,*]

[1]Department of Biomedical Engineering, University of California, Irvine, Irvine, CA 92697, USA

[2]Department of Neurobiology and Behavior, University of California, Irvine, Irvine, CA 92697, USA

[3]Center for the Neurobiology of Learning and Memory, University of California, Irvine, Irvine, CA 92697, USA

[4]Department of Psychiatry and Human Behavior, University of California, Irvine, Irvine, CA 92697, USA

[5]Comprehensive Epilepsy Program, Department of Neurology, University of California, Irvine, Irvine, CA 92868, USA

[6]Department of Neurological Surgery, University of California, Irvine, Irvine, CA 92868, USA

[7]Helen Wills Neuroscience Institute, University of California, Berkeley, Berkeley, CA 94720, USA

[8]Department of Psychology, University of California, Berkeley, Berkeley, CA 94720, USA

[9]Lead Contact

SUMMARY

How do we remember emotional events? While emotion often leads to vivid recollection, the precision of emotional memories can be degraded, especially when discriminating among overlapping experiences in memory (i.e., pattern separation). Communication between the amygdala and the hippocampus has been proposed to support emotional memory, but the exact neural mechanisms remain unclear. Here, we used intracranial recordings in pre-surgical epilepsy patients to show that successful pattern separation of emotional stimuli is associated with theta

*Correspondence: myassa@uci.edu (M.A.Y.), linjj@uci.edu (J.J.L.).

AUTHOR CONTRIBUTIONS

J.Z. collected, analyzed, and interpreted the data; R.F.S. collected the data and assisted with the analysis; B.A.M. interpreted the data; J.J.L., L.M., F.P.K.H., and S.V. managed patients and surgeries; J.Z., R.T.K., M.A.Y., and J.J.L. conceived the study, interpreted the data, and wrote the manuscript with input from all authors.

SUPPLEMENTAL INFORMATION

Supplemental Information can be found online at https://doi.org/10.1016/j.neuron.2019.03.025.

DECLARATION OF INTERESTS

The authors declare no competing interests.

DATA AND SOFTWARE AVAILABILITY

Freely available software and algorithms used for analysis are listed in the Key Resources Table. All custom scripts and data contained in this manuscript are available upon request from the Lead Contact.

band (3–7 Hz)-coordinated bidirectional interactions between the amygdala and the hippocampus. In contrast, discrimination errors (i.e., failure to discriminate similar stimuli) were associated with alpha band (7–13 Hz)-coordinated unidirectional influence from the amygdala to the hippocampus. These findings imply that alpha band synchrony may impair discrimination of similar emotional events via the amygdala-hippocampal directional coupling, which suggests a target for treatments of psychiatric conditions such as posttraumatic stress disorder, in which aversive experiences are often overgeneralized.

In Brief

Zheng et al. demonstrate that successful pattern separation of emotional stimuli is associated with bidirectional amygdalahippocampal interactions via theta band (3–7 Hz). In contrast, unidirectional influence from the amygdala to the hippocampus via alpha band (7–13 Hz) leads to overgeneralization errors (i.e., failure to discriminate similar stimuli).

INTRODUCTION

Emotion is a powerful modulator of episodic memory. Emotional events are thought to promote arousal during acquisition, which facilitates later recall (McGaugh, 2013). However, studies in humans have shown that the impact of emotion on memory is not always positive. We often remember the emotional gist but forget the details (Adolphs et al., 2005; Leal et al., 2014b). For instance, eyewitness testimony tends to focus on the weapon, while witnesses have impaired memory for other details of the crime scene and the perpetrator (Loftus et al., 1987). This emotional memory modulation can impair the discrimination of similar experiences, which is mediated by pattern separation (Leal et al., 2014a). This neural computation is critical for episodic memory and is vulnerable in neuropsychiatric disorders (Leal and Yassa, 2018). Therefore, the neural dynamics of emotional mnemonic discrimination not only are vital to understanding the biological basis of emotion and memory processing, but also provide circuit-level insights for understanding psychiatric illness, offering improved targeting of therapeutic interventions.

Although several hypotheses have been proposed to explain how emotional memories are processed in the human amygdala-hippocampal circuit (Phelps, 2004), the underlying neural mechanisms remain elusive. Prior brain imaging studies have suggested that the hippocampus plays a critical role in pattern separation (Leutgeb et al., 2007), while the amygdala modulates the strength of memory (Leal et al., 2014a). This division of labor is based on fMRI studies, which are limited by coarse temporal resolution and cannot inform on oscillatory modes of network communication to support emotional memory. In contrast, rodent neurophysiological studies show that low-frequency oscillations (3–13 Hz) reflect rhythmic fluctuations of membrane potentials and provide flexible temporal windows (Fries, 2005) to support interregional communication during aversive memory retrieval (Seidenbecher et al., 2003). High-frequency activity (HFA) (30–250 Hz) closely correlates with population spiking activity and likely reflects local neural processing. Coupling between the phase of low-frequency activity and the amplitude of HFA (i.e., phase-amplitude coupling [PAC]) has been proposed to modulate synaptic plasticity (Huerta and Lisman, 1995; Orr et al., 2001), flexibly organizing complex mnemonic information

(Heusser et al., 2016) to increase memory capacity (Inman et al., 2018; Lisman and Jensen, 2013) and promote adaptive learning (Stujenske et al., 2014), which requires highly detailed pattern-separated representations (McClelland et al., 1995). Here we use human depth electrode recordings with a high spatial and temporal resolution to test the hypothesis that low-frequency oscillations and HFA cooperatively facilitate amygdala-hippocampal interactions to support mnemonic discrimination of emotional stimuli in humans.

We recorded intracranial stereo-electroencephalography (SEEG) simultaneously from the amygdala and the hippocampus in 7 pre-surgical epilepsy patients while they performed an emotional pattern separation task (Leal et al., 2014b), in which participants were asked to distinguish among memories of similar emotional scenes (Figure 1A). This task has shown robust amygdala-hippocampal involvement in previous fMRI studies (Leal et al., 2014a, 2017), which reported that the amygdala response is elevated in emotional conditions regardless of mnemonic accuracy. In contrast to the fMRI studies, we observed that neural responses in both the amygdala and the hippocampus are modulated by both memory accuracy and valence. Specifically, correct discrimination of similar emotional stimuli was associated with bidirectional interactions between the amygdala and the hippocampus mediated by theta oscillations (3–7 Hz). In contrast, discrimination errors (i.e., failure to discriminate similar stimuli) were associated with alpha (7–13 Hz)-driven unidirectional influence from the amygdala to the hippocampus. These results highlight the complex oscillatory dynamics of amygdala-hippocampal interactions in facilitating retrieval of detailed emotional memories and provide a putative mechanism for emotional discrimination errors.

RESULTS

Emotion Interferes with Mnemonic Discrimination

Seven pre-surgical epilepsy patients (3 males and 4 females) (Table S1) performed an episodic memory task (Figure 1A) (Leal et al., 2014b). During encoding, subjects were instructed to rate the emotional valence (negative, neutral, or positive) of each picture. Immediately following encoding (~1 min), subjects performed a recognition test to categorize the repeated images as old and the first-seen images as new. To induce memory interference, lure items, which are similar to the ones presented in the encoding phase, were included in the recognition test, along with targets (i.e., repeated images) and foils (i.e., new images). All subjects performed well on the task (79.8% ± 1.8% accuracy, mean ± SEM; range = 73.1%−86.6%, Tables S1 and S2; chance level = 54.8%, $p < 0.05$, permutation test). We calculated the lure discrimination index (LDI) (Leal et al., 2014b) for each subject, operationalized as $p(\text{'New'}|Lure) - p(\text{'New'}|\text{Target})$, which corrected for the general tendency to reject items (Yassa and Stark, 2011) (e.g., calling an item new). This is analogous to the inverse of the corrected recognition score widely employed in a previous recognition memory test (Andersen, 2007). Similar to prior work (Kensinger and Schacter, 2007; Leal et al., 2014a, 2014b), performance significantly differed among positive, negative, and neutral stimuli $\left(F_{\text{valence} \times \text{LDI (subject number} \times 3)}\right.$ (2, 18) = 6.32, p = 0.008) (Figure 1B), with diminished LDI for emotional lures compared to the neutral ones (post hoc analysis, Scheffé test:

$d_{|Neg-Neu|} = 0.272, CV_{|Neg-Neu|} = 0.219,\ p < 0.01; d_{|P_{OS}-Neu|} = 0.171, CV_{|P_{OS}-Neu|} = 0.169,\ p < 0.05$

, where Neg, negative; Neu, neutral; and Pos, positive). The magnitude of the effect was larger for negative stimuli compared to positive stimuli, which might be due to the higher level of arousal elicited by the negative condition (Lang et al., 1993) (see Discussion).

Increased Theta Power and Decreased Alpha Power Predict Successful Mnemonic Discrimination

Local field potentials (LFPs) were recorded from the depth electrodes implanted in the amygdala (13 electrodes) and the hippocampus (17 electrodes) (Figure 1C). The localizations of depth electrodes were determined by three experienced raters (interrater reliability: $\kappa = 0.824$; see STAR Methods) based on the co-registered post-to pre-implantation MRI scans (post-computed tomography [CT] to pre-MRI for subject 7) and was guided by a high-resolution anatomical atlas, labeled with medial temporal lobe (MTL) sub-regions of interests (Figure S1). We examined neural responses while individuals performed memory recognition (processing period during the retrieval phase in Figure 1A), comparing correctly rejected (lure correct rejection [LCR]: lures correctly identified as new) versus incorrectly recognized (lure false alarm [LFA]: lures incorrectly identified as old) negative, neutral, and positive lures.

Both amygdala and hippocampal electrodes showed strong oscillatory activity peaking in the theta and alpha band range (3–13 Hz) (Figures 2A and 2B) during lure discrimination trials, which is consistent with previous findings of increased theta and alpha oscillations facilitating memory retrieval (Jutras et al., 2013; Seidenbecher et al., 2003). Furthermore, when we separated trials into LCR and LFA conditions (collapsed across valence) (Figure 2C), oscillations at distinct low-frequency bands reflected different task outcomes. Specifically, more prominent theta band (~2–7 Hz) activity was observed in both the amygdala and the hippocampus during LCRs, while more prominent alpha band (~7–14 Hz) activity was presented during LFAs ($p < 0.05$, corrected for multiple comparisons using the cluster-based permutation test; see STAR Methods) (Figure 2D). Moreover, the theta power increase and the alpha power decrease occurred simultaneously in the hippocampus (latency difference = 0.012 ± 0.004 s, $p = 0.421$), while the theta power increase led the alpha power decrease in the amygdala (latency difference = 0.824 ± 0.032 s, $p = 2.35e\text{-}7$). These dual frequency changes were only observed during lure discrimination (Figures S2A and S2B), with stronger theta power increases and alpha power suppression for LCRs compared to targets hits (i.e., targets correctly identified as old) and foil correct rejections (i.e., foils correctly identified as new) ($p < 0.05$, corrected using the cluster-based permutation test; see STAR Methods) (Figures S2C and S2D). We observed significant three-way interactions (emotion [negative, positive, and neutral], trial type [lure and foil], and accuracy [correct rejection and false alarm]) across theta and alpha power in both the amygdala and the hippocampus. Furthermore, significant emotion (negative, positive, and neutral) × accuracy (correct rejection and false alarm) interactions were observed in lures, but not foils, for these dual frequency changes in the amygdala and the hippocampus (Table S3). These results

suggest that the theta power increase and the alpha power decrease in the amygdala and hippocampus were spectral features specific to pattern separation.

Next, we examined the impact of emotional valence. Within each condition (LCR and LFA), trials were grouped based on each subject's valence ratings (negative, positive, or neutral) during the encoding session. The conditional power difference (LCR - LFA) was then calculated and averaged across time within the theta and alpha bands separately for different valences (negative, neutral, and positive). The theta and alpha bandwidths used in this analysis were determined by the significant clusters detected in Figure 2D (amygdala: AMY_{theta} = ~2–7 Hz, AMY_{alpha} = ~8–14 Hz; hippocampus: HPC_{theta} = ~2–6 Hz, HPC_{alpha} = ~7–13 Hz). We found the same spectral pattern (increased theta power during LCRs and increased alpha power during LFA s) across all three valence categories, indicating that theta and alpha oscillatory multiplexing served as a common mechanism for mnemonic discrimination irrespective of emotional valence. However, the magnitude of these conditional power differences was amplified by emotional valence in both regions ($AMY_{theta}: F_{valence\times trial}(2, 216) = 4.627, p = 0.011; AMY_{alpha}: F_{valence\times trial}(2, 216) = 7.934, p = 4.730e-4; HPC_{theta}: F_{valence\times trial}(2, 216) = 10.325, p = 5.211e-5; HPC_{alpha}: F_{valence\times trial}(2, 216) = 8.272, p = 3.461e-4$)

(Figure 2E), suggesting that a more robust oscillatory pattern is needed when discriminating similar emotional experiences compared to similar neutral ones. To ensure that these effects were not driven by the influence of evoked transients on the power estimation and the subsequent interpretation of directional analyses (Kovach, 2017; Wang et al., 2008), we assessed evoked response potentials (ERPs) for both LCR and LFA trials. This analysis showed no significant difference between conditions (Figure S3).

Theta and Alpha Amygdala-Hippocampal Synchrony Differentially Bias Discrimination Outcomes

Given the putative role of low-frequency oscillations in supporting interregional communication (Fries, 2005), we investigated low-frequency phase synchrony between the amygdala and the hippocampus. Instantaneous phases from both regions were extracted using the Hilbert transformation. Cross-regional coordination was quantified with phase locking values (PLVs), which measure the consistency of the phase relationship of each amygdala-hippocampal electrode pair (Lachaux et al., 1999). We computed PLVs up to 64 Hz at each time point to reveal the spatiotemporal dynamics of amygdala-hippocampal phase synchrony. After averaging across subjects, we found amygdala- hippocampal phase synchrony was evident in two frequency bands: early theta synchrony (~3–7 Hz), predicting LCRs, and later alpha synchrony (~7–13 Hz), associated with LFAs ($p < 0.01$, permutation test) (Figure 3A). This frequency-specific pattern was consistent at the individual level, with 6 of 7 subjects demonstrating theta synchrony for LCRs and alpha synchrony for LFAs (chi-square = 18.24, p = 0.006) (Figure 3B). In addition, such a frequency difference between the two conditions was consistent across different emotional conditions (Figure 3C), and the strength of conditional differences (LCR versus LFA) of theta or alpha band synchrony was enhanced for emotional trials versus neutral ones (neutral < positive < negative; theta synchrony: $F_{valence \times trial}$ (2, 216) = 5.621, p = 0.004, post hoc analysis, Scheffé test, $d_{|Neg-Neu|} = 0.400, CV_{|Neg-Neu|} = 0.327, p = 2.241e-3$; alpha synchrony:

$F_{\text{valence}\times\text{trial}}(2, 216) = 4.212, p = 0.016$, post hoc analysis, Scheffe test, $d_{|Neg-Neu|} = 0.356, CV_{|Neg-Neu|} = 0.288, p = 1.826e-3$) (Figure 3D). The outcome selectivity was not attributed to local power differences (Kovach, 2017): frequency-specific interregional synchrony remained significant even when computed using the trials with balanced theta and alpha power across LCRs and LFAs (n = 133 trials, $p < 0.01$, permutation test) (Figures S4A and S4B). To reduce sensitivity to volume conduction and uncorrelated noise, we conducted phase synchrony using the weighted phase lag index (WPLI) (Vinck et al., 2011), which validated the prediction power of theta and alpha synchrony for subjects' behavioral outcomes (Figure S4D). Moreover, although increased theta phase synchrony was observed in the foil trials (Figure S5A), the significant emotion × accuracy interactions were observed only in lures, not in foils (Table S4), providing evidence that the emotional modulation of theta and alpha phase synchrony is specific to pattern separation.

Bidirectional Amygdala-Hippocampal Interactions Support Mnemonic Discrimination

We used frequency-domain Granger causality analysis to quantify interregional directional influence, which measures the degree to which the signal from one region can be better predicted by incorporating information from the other. We found that the direction of influence differed between conditions, with theta-driven bidirectional interactions for LCRs and alpha-driven unidirectional influence from the amygdala to the hippocampus for LFAs ($p < 0.01$, permutation test) (Figure 4A). Moreover, this directional influence was specific to lure trials: no significant directional interactions between the amygdala and the hippocampus were observed during foil trials (Figure S5B). These conditional differences remained significant when band-specific LFP power was balanced across LCRs and LFAs (Figure S4C), indicating that the observed frequency-specific directionality was not due to differences in local power. During LCRs, directional influence in the theta band from the amygdala to the hippocampus was amplified by emotion (negative > positive > neutral; $F_{\text{valence} \times \text{ Granger causality index (subject number} \times 3)}(2, 18) = 5.084,\ p = 0.018$) (Figure 4B, top), while the reciprocal influence from the hippocampus to the amygdala remained constant ($F_{\text{valence} \times \text{Granger causality index (subject number} \times 3)}$ (2, 18) = 2.976, p = 0.076) (Figure 4B, top), suggesting that successful discrimination of similar emotional stimuli involved an enhanced engagement of the amygdala to overcome emotional interference. In contrast, for LFAs, the network is dominated by the greater influence from the amygdala to the hippocampus in the alpha band compared to the reverse direction, which is consistent across negative, positive, and neutral valence ($F_{\text{valence} \times \text{Granger causality index (subject} \times 3)}$ (2, 18) = 2.268, p = 0.132) (Figure 4B, bottom). These results suggest that successful discrimination of overlapping memories (for all three valence groups) requires bidirectional information exchange in the amygdala-hippocampal circuit.

Distinct Theta Phases Encode Information from the Amygdala and Hippocampus

PAC is an important mechanism to flexibly coordinate interregional information transfer, with the phase of slow oscillations dynamically modulating the amplitude of HFA (Helfrich and Knight, 2016). This mechanism has been shown to support phase-dependent encoding of different mnemonic representations (Heusser et al., 2016; Watrous et al., 2015). We performed cross-regional PAC in both phase-amplitude combinations (low-frequency phase

from the amygdala and high-frequency amplitude from the hippocampus, and vice versa) using the electrode pairs exhibiting the most significant low-frequency phase synchrony (Zheng et al., 2017). The interregional influence was quantified as the correlation between low-frequency (2–32 Hz) phases from one region (i.e., the modulating signal) and the amplitude of HFA (30–250 Hz) from the other (i.e., the modulated signal). Again, frequency-specific features emerged in interregional PACs between the amygdala and the hippocampus for LCRs, with the theta phase of the amygdala entraining the HFA of the hippocampus (~70–130 Hz, peaked at 93 Hz) and the theta phase of the hippocampus modulating the HFA of the amygdala (~60–140 Hz, peaked at 84 Hz). In contrast, for LFAs, the alpha phase of the amygdala was found to modulate hippocampal HFA (~45–125 Hz, peaked at 112 Hz) (Figures 5A and 5B). To address whether the low-frequency phase drives the amplitude of HFA, or vice versa, we performed the cross-frequency directional analysis. Because the signal-to-noise ratio (SNR) varies across frequency bands and Granger causality analysis is sensitive to SNR (Cohen, 2014), we re-assessed the interregional directionality between low-frequency oscillations (i.e., theta and alpha) and HFA using the phase slope index (PSI) (Nolte et al., 2008). We found that PSI differed between the two conditions, with a bidirectional, theta phase-driven network during LCRs and a unidirectional, amygdala-alpha phase-driven network during LFAs ($p < 3.212 \times 10^{-12}$, permutation test) (Figures 5C and 5D). These results not only confirmed the directional interactions observed from the Granger causality analysis but also suggested that such directional influence could shape HFA, an index of local neural activity, via PAC.

Because low-frequency oscillations are thought to organize cell assemblies to encode distinct information (Lisman and Jensen, 2013), we then asked whether a specific phase of the low-frequency oscillation was co-modulated with HFA in a behaviorally relevant manner, analogous to spike and phase coupling, in which local neuronal spiking is biased according to the oscillatory phase of the LFP (Buzsaki et al., 2012). Given that the SNR strongly depends on the strength of oscillatory modulation (Watrous et al., 2015), we bandpass-filtered the modulating signals within the frequencies demonstrating the strongest modulation effect (extracted from Figures 5A and 5B) and examined when HFA from the modulated signals occurred relative to the phases of the modulating signal. A phase-dependent coding mechanism emerged in single-trial examples (shown in Figure 5E) and was confirmed by group analysis across all subjects and trials (Figure 5F). Specifically, for LCRs, HFA from both the amygdala and the hippocampus was modulated by the theta oscillations around the trough (average amygdala HFA occurred at 157°, $p_{\text{Amygdala}} = 1.05 \times 10^{-4}$, Rayleigh test; average hippocampal HFA occurred at 202°, $p_{\text{Hippocampus}} = 2.33 \times 10^{-5}$, Rayleigh test), with HFA from the amygdala and hippocampus separately occurring at the descending and ascending slope, respectively (pattern classification methods, $p < 10^{-8}$, binomial test; see STAR Methods). In contrast, for LFAs, the occurring phases of HFA from both sides were largely overlapping (pattern classification methods, $p > 0.05$, binomial test) and were distributed across different alpha phases ($p_{\text{Amygdala HFA}} = 0.068$, $p_{\text{Hippocampus HFA}} = 0.082$, Rayleigh test). Moreover, for LCRs, the overlapping ratio between the occurring phases of the amygdala and the hippocampal HFA differed across emotional valences ($F_{\text{valence} \times \text{phase overlapping ratio (subject number} \times 3)}(2, 18) = 4.062$, $p = 0.035$), with greater overlap for the emotional stimuli compared to the neutral trials. However, for LFAs, the

overlapping ratio remained the same across all valence groups ($F_{\text{valence} \times \text{phase overlapping ratio (subject number} \times 3)}$ (2, 18) = 2.205, p = 0.139) (Figure 5G). Such phase-dependent coding provides a putative oscillatory mechanism that may increase the coding capacity of the amygdala-hippocampal circuit, with different phases reflecting distinct information (Heusser et al., 2016; Lisman and Jensen, 2013; Watrous et al., 2015). In summary, the amygdala and the hippocampus use frequency- and phase-specific oscillatory mechanisms to optimize bidirectional information transfer, with HFA at the trough phase of theta oscillations predicting successful mnemonic discrimination.

DISCUSSION

We provide evidence that interregional communication between the amygdala and the hippocampus, using specific oscillatory modes of frequency, directionality, and phase information, supports successful mnemonic discrimination of emotional events. In particular, bidirectional theta oscillations in the amygdala-hippocampal circuit are enhanced during LCRs, with HFA in both regions nested at distinct phases around the theta trough (Figure 6). Furthermore, this oscillatory pattern is driven by a stronger theta power when successfully discriminating similar emotional experiences, indicating that a more robust oscillatory communication is needed to prevent discrimination errors. In contrast, enhanced alpha power, driven by the amygdala, is associated with theta power decreases in both the amygdala and the hippocampus during LFAs. The latter observation suggests that the amygdala exerts a unidirectional influence on the hippocampus via increased interregional alpha synchrony, providing a novel mechanistic account for discrimination errors in memory, which may underlie pathological remembering in conditions such as post-traumatic stress disorder (PTSD).

These interregional oscillatory dynamics are consistent with known structural connections between the amygdala and the hippocampus. Because of our surgical technique of aiming the depth electrode in a superior trajectory to access the inferior amygdala above the tentorium, all of our electrodes targeting the amygdala were located in the basolateral nucleus. Amaral and Cowen demonstrated that in nonhuman primates, retrograde tracers from the hippocampal formation were predominately found in the anterior amygdaloid area, including the basolateral nucleus (Amaral and Cowan, 1980). A subsequent study by Ste-fanacci and colleagues showed that the perirhinal and parahip-pocampal cortices (which are strongly interconnected with the hippocampus) have robust bidirectional connections with the basolateral nucleus (Stefanacci et al., 1996). Our results suggest that the functional connectivity of the hippocampal-basolateral nucleus could be dynamically modulated by pattern separation signals.

Low-frequency oscillations (3–13 Hz) in the MTL are thought to play a critical role in successful memory encoding (Hasselmo and Stern, 2014) and retrieval (Seidenbecher et al., 2003). In particular, enhanced theta power during LCRs is consistent with the well-established role of theta oscillation modulation of amygdala-hippocampal synaptic plasticity (Bazelot et al., 2015; Huerta and Lisman, 1995; Orr et al., 2001) to flexibly organize complex mnemonic information via theta-gamma phase coding (Heusser et al., 2016). Moreover, increased theta power was associated with decreased alpha power, suggesting that

synergy between theta power increases and alpha power decreases supports mnemonic discrimination. Previous studies have shown that decreased alpha power in the hippocampus is associated with successful memory retrieval (Staresina et al., 2016), consistent with our results. In the cortex, decreased alpha power is correlated with an increase in HFA power and firing rates and has been associated with improved cognitive processing (Bahramisharif et al., 2018; Bastos et al., 2018; Haegens etal.,2011; Lundqvistetal., 2016; Miller etal., 2018). In contrast, increased alpha power is linked to decreased HFA power and neuronal spiking and poor discrimination performance. These findings suggest that alpha oscillations are correlates of rhythmic inhibition, possibly providing top-down executive control to gate information flow (Cooper etal., 2003; Hanslmayret al., 2007; Kli- mesch et al., 2007; Min and Herrmann, 2007; Pfurtscheller, 2001). Considering our results and these works, we suggest that the theta power increases and the alpha power decreases facilitate amygdala and hippocampal processing during mnemonic discrimination by organizing neural activity (theta) and selectively filtering task-relevant information to attend to emotional information (alpha) (Jokisch and Jensen, 2007; Miller et al., 2018; Nerad and Bilkey, 2005; Parish etal., 2018; Sauseng et al., 2005; Staresina et al., 2016). Alpha power increases are also observed during the processing of emotional stimuli in other studies (Güntekin and Basar, 2014) and the magnitude of alpha power increases with the stimulus's arousal level (Aftanas et al., 2002), possibly serving an important adaptive function of sharpening attention to emotional stimuli (i.e., threat detection). The role of alpha power increases in the detection of emotional stimuli may come at the cost of the precise theta-gamma phase coding (Heusser et al., 2016; Lisman and Jensen, 2013) required for mnemonic discrimination to favor knowledge critical for survival. The result is that information about threats may be overgeneralized. For example, if someone is bitten by a dog, he or she may become anxious around dogs of all breeds and sizes, i.e., generalization at the cost of discrimination.

An alternative explanation of the role of theta and alpha oscillations in the MTL is that these rhythms may exist on a continuum, with the frequency modulated by the rate of environmental exploration. Whereas several studies have observed a slower theta rhythm (3–7 Hz) in humans during virtual navigation (Ek- strom et al., 2005) and memory tasks (Axmacher et al., 2010), more recent studies in freely moving humans have demonstrated the presence of a high theta band (8–13 Hz, also referred to as an alpha band) that is similar to the oscillations observed in freely moving rodents (Bohbot et al., 2017; Bush et al., 2017; Aghajan et al., 2017). This high theta increased in prominence with movement speed, as well as the rate of exploration (Aghajan et al., 2017), suggesting a role in active sensing and encoding the environment. We speculate that alpha band oscillations, which appear to gate unidirectional influence from the amygdala on the hippocampus and enable false recognition of negatively va-lenced information are functionally similar to the high theta oscillations noted in studies in freely moving humans (Bohbot et al., 2017; Bush et al., 2017; Aghajan et al., 2017), as well as in studies of saccade-based environmental exploration in monkeys (Jutras et al., 2013). By this account, higher frequency theta and alpha oscillations could be related to a higher sampling rate of emotional stimuli. This is consistent with an evolutionary account in which the amygdala's influence is thought to orient the hippocampus to emotional events in the environment and perhaps generate an overgeneralization response (i.e., false alarm to similar negative experiences) that is

adaptive, especially if the stimulus has the potential to threaten survival. This can be thought of as a rapid override system that is related to active sensing or alert exploration. These results further demonstrate the potential functional heterogeneity of different theta and alpha oscillations in the MTL.

During LCRs, the strength of theta synchronization and alpha desynchronization is amplified by emotion (Figures 2E and 3C). Previous studies have shown that increased theta synchronization correlates with memory load and task difficulty (Jacobs et al., 2006) while alpha desynchronization increases corresponding to the amount of distracting information (Sauseng et al., 2005). Because emotional stimuli can bias attention to allocate more resources for the processing of emotional stimuli (Taylor and Fragopanagos, 2005), it is possible that when discriminating similar emotional experiences, stronger distracting emotional signals need to be suppressed by higher levels of alpha desynchronization. At the same time, task-relevant mnemonic signals may need to be strengthened by theta to increase SNR. This emotional modulation of mnemonic oscillatory dynamics is not independent of valence. We observed that negative valence is associated with a greater magnitude of theta synchronization and alpha desynchronization during LCRs when compared to the positive ones. One possible explanation for these results is that negative and positive stimuli are not matched for arousal. Prior studies have also shown that this matching is difficult to accomplish because negative stimuli, in general, tend to induce higher levels of arousal compared to positive stimuli (Lang etal., 1993). In addition, the amygdala does not solely respond to emotional stimuli but also prioritizes emotional information such as reward, motivation, and socially relevant events (Morrison and Salzman, 2010). Neutral stimuli in our study also elicited amygdala-hippocampal interactions that were modulated with valence. That said, understanding how positive and negative valences influence oscillatory dynamics is an important facet of emotional memory that, if better understood, may have therapeutic potential to reverse the negativity bias often observed in patients with mood disorders (Leal and Yassa, 2018). The stronger effect in the negative trials might also be influenced by the unbalanced social information in the stimuli set, such as a greater number of faces present in the negative stimuli. If this is the case, it would indicate that the amygdala facilitates the integration of socially relevant information for mnemonic discrimination. Future studies regarding the interactions between social and emotional dimensions could provide a more precise model of how social-emotional information influences mnemonic discrimination.

Our results suggest that impaired discrimination of emotional experience might result from an amygdala-driven amplification of emotional processing via enhanced amygdala-hippocampal alpha synchrony, which may lead to false alarms to similar negative experiences (i.e., failure to discriminate or form highly specific representations of negative experiences), which is common in psychiatric disorders such as PTSD. Our findings provide a neural mechanism underlying this phenomenon and propose a circuit-level framework for possible neuropsychiatric therapy, such as deep brain stimulation, transcranial alternating current stimulation, and transcranial magnetic stimulation (Zheng and Lin, 2018). Moreover, studies (Grossman et al., 2017) in mice using temporally paired electrical fields to entrain hippocampal oscillatory activity without recruiting the overlying cortex suggest new possibilities for noninvasive stimulation of deep brain structures. Although scaling the

approach and technology safely to humans will be challenging, it is conceivable to use such stimulation techniques in humans. Specifically, one might be able to disrupt alpha synchrony (e.g., cancel out the alpha wave by stimulating with the same frequency but opposite phase) and boost theta synchrony (e.g., enhance theta phase alignment) during aversive memory retrieval to noninva- sively correct discrimination errors in patients with PTSD (Zheng and Lin, 2018). In addition, a study has shown that direct electrical stimulation of the amygdala can enhance declarative memory in humans, possibly via increased theta and gamma PAC (Inman et al., 2018). The overgeneralization behavior in patients with PTSD evolves over long periods, instead of the short delay (i.e., a couple of minutes) used in current task design. In addition, other brain regions, such as the prefrontal cortex, may play critical roles as part of this emotional memory circuit. Thus, future studies examining more brain regions and across longer timescales are needed to understand the putative mechanisms underlying overgeneralization in patients with PTSD. The current study was conducted with patients with epilepsy, whose brains may undergo epilepsy-related changes. However, behavioral outcomes from the patients closely match those of healthy volunteers. Furthermore, in line with recommendations of a review from human and nonhuman primate intracranial researchers, we excluded trials associated with seizures and epileptiform discharges, as well as recordings from epileptic tissues (Parvizi and Kastner, 2018).

In summary, we report evidence of novel electrophysiological signatures of emotional memory in the amygdala-hippocampal network, which is implicated in a host of neuropsychiatric diseases and memory deficits. Understanding these neural mechanisms provides a critical framework for developing circuit-specific intervention in people with disordered memory and emotion (Gordon, 2016).

STAR★METHODS

CONTACT FOR REAGENT AND RESOURCE SHARING

Further information and requests for resources and reagents should be directed to and will be fulfilled by the lead contact, Michael A. Yassa (myassa@uci.edu).

EXPERIMENTAL MODEL AND SUBJECT DETAILS

Participants—Data were obtained from epilepsy patients undergoing intracranial EEG monitoring at the University of California, Irvine, Medical Center to localize epileptic foci for potential surgical resection. Intracranial depth electrodes (Integra or Ad-Tech, 5-mm inter-electrode spacing) were stereotactically implanted with robotic assistance (Rosa Surgical Robot, Medtech, New York, NY). The electrode placements were exclusively guided by clinical needs. Before testing, all subjects gave informed written consent in accordance with the Institutional Review Board of the University of California, Irvine. Patient selection was based on the following inclusion criteria: 1) having electrodes in both the amygdala and the hippocampus contralateral to or outside of the epileptogenic region; 2) meet the task performance criteria with accuracy rates above 70% (Table S1). In total, 12 patients participated in the task. Two subjects were excluded because of low accuracy rate (56.7% and 64.4%) and 3 subjects were excluded because electrodes in the amygdala and/or

hippocampus region coincided with the epileptogenic zone. The remaining 7 subjects (4 Female, 3 Male, Age 21–58, Table S1) were included in this study.

METHOD DETAILS

Electrode localization—Electrodes were localized in each subject using co-registered pre-implantation and post-implantation structural T1-weighted MRI scans except S5, who only had post-implantation CT scans. First, we registered post-implantation scans to the pre-implantation scans using a six-parameter rigid body transformation (three rotations and three translations in x-z directions), which was implemented in Advanced Normalization Tools (ANTs http://stnava.github.io/ANTs/). Then a high-resolution anatomical template (an ultrahigh-resolution structural MPRAGE scans collected in our previous study and standardized to MNI space (Leal et al., 2014a), 0.55mm isotropic resolution, 273 sagittal slices, field of view = 240 × 240 mm, flip angle = 9o, TR/TE = 13/5.9ms, matrix size = 448 × 448, inversion pulse TI = 1110ms), with labels of medial temporal lobe subfields was applied to guide our localization for each electrode. The labeled template was resampled (1mm isotropic) and aligned to each subject's pre-implantation scans using ANTs Symmetric Normalization (Avantset al., 2011). Based on the anatomical labels within each subject's space, the electrode location was determined by identifying the region of interest that encompassed the center of the electrode artifacts. The electrode localization was performed by three experienced raters independently. The inter-rater reliability is 0.824 (function *Kapam.fleiss* from R statistical tool). All the electrodes included in the analyses have consistent results from at least two raters. The electrode localization results and the selection of re-referencing electrodes within white matter were furthered reviewed by the epileptologist (J.J.L.).

Experimental design—Participants viewed a series of images at the center of a laptop screen with a black background. The stimulus set consisted of novel scenes freely available online. All the images were rated for emotional valence and similarity (scale from 1 to 8, with 1 indicating the least amount of similarity and 8 indicating that the items were identical) in orthogonal experiments with separate samples. Specifically, for the similarity ratings, an independent group (N = 31, 21 female, age 19 ± 1,) was used to examine relative similarity of each stimulus. We presented pairs of stimuli (the original image presented during study and its similar lure) side-by-side and collected their subjective similarity ratings scaled from 1 to 8 (1 indicating the least amount of similarity and 8 indicating that the items were identical). We controlled the similarity ratings for lures across different emotional group (Leal etal., 2014b). Detailed information about the supplementary rating studies in the separate similarity rating participants can be found in the previous paper (Leal etal., 2014b). In addition, emotional images are often related thematically while neutral pictures may cover broader themes (Talmi and Moscovitch, 2004). If this was the case, we might expect that similarities across emotional items higher than similarities across neutral ones. To address this issue, we assessed similarities within stimuli across valence, based on similarity ratings from an independent group of participants (27 participants, 11 females; via Amazon Mechanical Turk). To ensure the quality of online ratings, participants were asked to complete only one session per day (~1.5 hours). In addition, we randomly inserted 5% of control trials with two identical images in the task to track participants' behavioral

performance throughout the session. Only participants with greater than 95% accuracy for these control trials were included (4 participants were excluded due to their low behavioral performance). Based on the online ratings, we found no significant difference across valence ($Similarity_{negative}$ = 5.47 ± 0.13, $Similarity_{positive}$ = 5.39 ±0.11, $Similarity_{neutral}$ = 5.64 ± 0.14, $p > 0.05$); no significant difference across trial type ($Similarity_{target}$ = 5.68 ± 0.12, $Similarity_{lure}$ = 6.21 ± 0.28, $p > 0.05$); and no significant interaction ($p_{pvaience \times trial\ type} > 0.05$).

During the encoding phase, 148 images were presented in pseudorandom order and subjects were instructed to rate the emotional valence of each stimulus ('negative', 'neutral' or 'positive'). After a short delay (~1 minute), subjects were exposed to 290 images including target (repeated images, n = 54), lure (similar images, n = 97) and foil items (new images, n = 139). The lure items were evenly distributed across emotional valence (NegLure = 33; NeuLure = 32; PosLure = 32) and similarity level (NegSIM = 6.29 ± 0.11; NeuSIM = 6.14 ± 0.12; PosSIM = 6.41 ± 0.08, $p > 0.05$). During the test period, subjects were asked to identify whether each image was shown in the encoding phase or not. Subjects needed to make the response via key press within the 2 s time window and the trials where subjects failed to make a decision within the time period (< 2%) were excluded from the analysis.

Notably, the stimuli have balanced visual attributes: including balanced image size, luminance, contrast, complexity, entropy, and color composition across all three valence groups (Table S4; each visual attribute was calculated using the same method from a published image dataset, "Nencki dataset" (Marchewka et al., 2014). Moreover, the stimuli have balanced brightness ($p_{theoritical}$ = 0.243 and $p_{human\ vision}$ = 0.187) and color tone (82.2% negative images, 91.1% positive images and 94.2% neutral images were rated as color balanced) across all three valence groups (Figure S6) as well based on the theoretical calculations and ratings from an independent group (11 participants, 4 females) via Amazon Mechanical Turk.

Data acquisition and preprocessing—Stimuli were presented using PsychoPy2 (Version 1.82.01) software (Peirce, 2009) on an Apple MacBook Pro, which was placed on the service tray at a comfortable distance in front of participants. An external Apple keyboard was used to capture subjects' responses. Intracranial EEG data were acquired using a Nihon Kohden recording system (256 channel amplifier, model JE120A), analog-filtered above 0.01Hz and digitally sampled at 5000Hz. After data acquisition, the preprocessing of raw data was conducted using customized MATLAB scripts. First, neural recordings were down sampled at 2000Hz and band-pass filtered between 1 to 250Hz using the zero phase delay finite impulse response (FIR) filter with Hamming window. Then power spectral density (PSD) was estimated using Welch's method (pwelch,m in Signal Processing Toolbox from MATLAB). Line noises (usually 60Hz and its harmonics) inspected from PSD plots were removed via the multi-taper regression method. Based on the electrode localization results, channels in the amygdala and the hippocampus were re-referenced to the nearest white matter electrodes on the same depth electrode probe. The epileptiform discharges were manually marked (using databrowser.m in FieldTrip; Oostenveld et al., 2011) by the epileptologist (J.J.L.), who was blinded to electrode locations and trial information (e.g., stimuli onsets and subject's performance). Importantly, there

were no seizures recorded in any subject while performing the task, and only the electrodes contralateral to or outside of the seizure onset zone were included in the analyses.

QUANTIFICATION AND STATISTICAL ANALYSIS

Behavioral analysis—First, we evaluated subject's task performance by computing the accuracy rate overthe test phase (i.e., the ratios between the total number of correct trials and the total number of responded trials) across all conditions (Table S1) and for individual stimuli types (Table S2). Then we quantified their discrimination ability by calculating the LDI, which is the difference between the number of lure correct rejections and target miss: $p('New'|Lure) - p('New'|Target)$ for each valence group. To more accurately reflect subjects' perception of emotional valence, we used subjects' own ratings (97.2% consistent with the ratings from an independent group) during the encoding session to group trials into different valence conditions.

Event-related potentials—We then segmented the preprocessed intracranial recordings into event-related epochs, including a 500ms pretrial baseline and a 2000ms time window after trial onset. The segmented data were zero-padded to minimize filter-induced edge effects and were low-pass filtered at 30Hz using a finite impulse response filter (eegfilt.m function in EEGLAB toolbox; Delorme and Makeig, 2004). Task-induced ERPs were calculated within each condition (lure correct rejection versus lure false alarm) by averaging across filtered epochs and normalized to the averaged signal across the pre-trial baseline period. A two-sample t test was performed for each data point to determine the significant difference between conditions (t test, $p > 0.05$). To remove the potential contribution of signal components phase-locked to the trial onset (e.g., ERPs), calculated ERPs were subtracted from each channel before further analysis.

Frequency decomposition and task-induced power—Time-frequency representations of power were computed for each event-related epoch, with FIR filtering between 1 to 250Hz through 28 logarithmically spaced frequencies. The adaptive bandwidths ensured precise phase estimations within narrow bands of low-frequency oscillations while the broader range of higher-frequency eliminated sideband effects and prevented spurious PAC (Aru et al., 2015). We then applied the Hilbert transform (hilbert.m function in Signal Processing Toolbox from MATLAB) to extract analytic amplitude and phase for all filtered traces. The task-induced power (2–250 Hz) was calculated by squaring the analytic amplitude envelope and was normalized to the pre-trial baseline using relative change in decibel conversion (dB). Results shown in Figure 2C were averaged across all the subjects. Notably, the time-resolved power estimation is inherently temporally smoothed, especially for low frequencies (in the order of hundreds of milliseconds), which could contribute to smearing effect onsets earlier in time. To examine whether the task-induced power change reflected different task outcomes, we quantified the significance of the power difference between the lure correct rejections and lure false alarms and corrected for multiple comparisons using cluster-based permutation test (Function *ft_timelockstatistics* from Fieldtrip toolbox). Specifically, for every data sample ((channel, frequency, time)-triplet), the power difference between the lure correct rejections and lure false alarms was quantified by means of a t-value. Samples with t-values above the threshold (2.5^{th} and 97.5^{th}

quantiles for the two-sided t test) were selected and were clustered in connected sets on the basis of temporal, spatial, and spectral adjacency. This empirical dataset was then compared to a Monte Carlo distribution, which was created by shuffling the conditional labels for 1000 times. Conditional power differences were considered significant when the maximum of the cluster-level summed t-values in the empirical data exceeded the threshold (i.e., 95th percentile of the maximum of the cluster-level summed t-values) of the null distribution. As shown in Figure 2D, significant power increase (lure correct rejection > lure false alarm) and power decrease (lure correct rejection < lure false alarm) were highlighted by black and white curves respectively. Notably, similar analyses were also conducted when comparing the power difference between the lure correct rejections versus target hits or foil correct rejections (Figure S2).

Inter-regional phase synchrony—The strength of inter-regional neural synchrony was quantified by the PLV (Lachaux et al., 1999), which calculates the phase d differences between two channels (a, b) averaged across trials for a given time point t and frequency f:

$$PLV(t,f) = \frac{1}{Ntrials}\left|\sum_{n=1}^{n=Ntrials} \exp\left(i\left[\theta_{n,a}(t,f) - \theta_{n,b}(t,f)\right]\right)\right|$$

It measures the degree of consistency for each electrode pair phase relationship independent of their absolute phases and amplitudes - among repeated trials, with values approaching 1 referring to small variations across trials and strong phase synchrony between two channels. We performed the PLV analysis for each electrode pair, including all possible electrode pairs (one electrode from the amygdala and one from the hippocampus), within the retrieval processing period (2 s time window after stimuli onset). Then we grouped individual $PLV(t, f)$ spectrogram according to different conditions (lure correct rejection versus lure false alarm as shown in Figure 2A; negative, positive, and neutral as shown in Figure 2C). To test the statistical significance of PLV, a null distribution was created by randomly shuffling the signal from each electrode pair, computing the corresponding PLV spectrograms and repeating the same procedure for 1000 times. Then we averaged the null distribution of all electrode pairs and compared the observed averaged PLV with this averaged null distribution. The results shown in the right panel of Figure 3A were depicted with P values (e.g., P - 0.05 observed data exceed 95% surrogate data), with warmer colors denoting greater significance levels. To improve visualization, the PLV spectrogram plots were smoothed using a cubic spline interpolation method (spline.m function in MATLAB). Similar to power estimates, the PLV results were temporally smoothed, which may result in smearing effect with earlier onset relative to stimulus onset.

Weighted phase lag index (WPLI)—We further confirmed the amygdala-hippocampal phase synchrony results using weighted phase lag index (WPLI), which is less sensitive to the volume conduction driven by a single or common source (Vincket al., 2011). WPLI is based on the imaginary component of the cross-spectrum between two signals, which reflects the conduction delay and is more reliable to detect the true neural interactions. WPLI is defined as:

$$\mathrm{WPLI} = \frac{\left|\sum_{n=1}^{N} \Im\{X_n\}\right|}{\sum_{n=1}^{N} \left|\Im\{X_n\}\right|}$$

In which, $\Im\{x_n\}$ denotes the imaginary component of the cross-spectrum in the nth trial and N is the total trial number. Thus, for each condition (lure correct rejection and lure false alarm), we conducted WPLI for each amygdala-hippocampal electrode pair (across all possible amygdala hippocampal electrode pairs) using function ft_connectivity_wpli.m from Fieldtrip Toolbox. To assess the significance level of WPLI-based phase synchrony measurements, we conducted similar permutation test as described in the "interregional phase synchrony" section by generating null distribution based on 1000 shuffled datasets. The results shown in the Figure S4D were depicted with z scores (z = 5.32 equals to P = 0.05, which means that observed data precede 95% surrogate data), with warmer colors denoting greater significance levels. For better visualization, the WPLI spectrogram plots were smoothed using a cubic spline interpolation method (spline.m function in MATLAB). WPLI results are temporally smoothed, which may contribute to smearing effect as power estimates and PLV results.

Phase amplitude coupling and phase slope index—PAC was computed for the amygdala-hippocampus electrode pair with the strongest inter-regional phase synchrony in each subject within the retrieval processing period (the 2 s time window after the stimuli onset) and was calculated as the phase coherence between the low-frequency oscillation and the low-frequency filtered HFA (methods have been described in the previous paper (Zheng et al., 2017)). The directionality within each electrode pair with the strongest inter-regional phase synchrony in each subject was quantified as Phase Slope Index (PSI) (Nolte et al., 2008), which estimates the slope of the phase differences between the modulating (sender) and modulated (receiver) signals as a function of frequency. By applying the PSI to the phase of low-frequency (f) oscillations and the amplitude envelope of high-frequency (v) activity, the directional index can be defined as:

$$\psi(f) = Im\left(\sum_{f-\frac{\beta}{2}}^{f+\frac{\beta}{2}} C^*(v,f)C(v,(f+\delta f))\right)$$

where $C(v, f)$ is the complex coherency as the normalized cross-spectra between two time series and Im denotes the imaginary part. Since the transmission between modulating and modulated signal has a fixed time delay, the phase spectrum between these two signals will change systematically as a function of frequency. In other words, when the phase differences increase with the corresponding frequencies, a positive slope of phase spectrum is expected, suggesting that low-frequency phases lead the high-frequency amplitude. On the other hand, a negative PSI refers to the opposite directionality. The statistical analysis of cross frequency PSI is similar to the method described in the section 'Interregional phase synchrony', by randomly shuffling the trials 1000 times. The PSI null distribution was calculated using

shuffled low-frequency phase and high-frequency amplitude. The 95th percentile of the surrogate data was defined as the significant threshold. For better visualization, the PSI spectrogram plots were smoothed using a cubic spline interpolation method (spline.m function in MATLAB).

Granger causality analysis—To confirm the directionality between the amygdala and the hippocampus, we computed spectral Granger causality, which quantifies the prediction error of the signal in the frequency domain by introducing another time series. Before fitting to the multivariate autoregressive model to compute the spectral Granger causality, the time series data from each amygdala-hippocampal electrode pair with the strongest inter-regional phase synchrony in each subject were low-pass filtered at 85 Hz, down-sampled to 250 Hz and normalized within each trial (e.g., subtracting the temporal mean and cross-trial mean). Then, we defined the model order using the Multivariate Granger Causality (MVGC) Toolbox based on the Akaike information criterion. The model order for each subject varied from 8 to 15. The Granger causality index was computed within the retrieval processing period (2 s time window after stimuli onset) for both directions (amygdala to hippocampus, hippocampus to amygdala). The significance level testing for Granger causality is the same method used in the section 'Interregional phase synchrony' by randomly shuffling the trials 1000 times. Then the Granger causality null distribution was created and the 95th percentile of the surrogate data was defined as the significant threshold.

Pattern classification analysis—To test whether the phase of theta or alpha oscillations time-locked to the stimulus evoked HFA could decode distinct directional information, we performed a pattern classification analysis. As shown in Figure 5E, HFA occurred at different phases of the low-frequency oscillations. We used these occurring phase of HFA relative to its modulating frequency (lure correct rejection: theta oscillations; lure false alarm: alpha oscillations) as the input of the classifier. The output of the classifier was the prediction of task outcomes for each high-frequency event. Similar to previous studies (Lopour et al., 2013; Watrous et al., 2015), we chose a linear classifier and converted phase values as a vector quantity in the complex plane, with cosine and sine of the phase referring to the real and imaginary part respectively. The classifier was calculated by determining the sums for lure correct rejections and lure false alarms and taking the difference between the two conditions. Then, we projected the phase from new trials onto the classifier by taking the dot product in each direction:

$$q = \int_0^1 \cos\theta(t)\left(\varphi_{real\ jncorrect}(t) - \varphi_{real,\,corect}(t)\right) dt + \int_0^1 \sin\theta(t)\left(\varphi_{imag,\,incorect}(t) - \varphi_{imag,\,correct}(t)\right) dt$$

We quantified the differences for the projection distributions between lure correct rejection q_{CR} and lure false alarm q_{IC} conditions using the discriminability index d:

$$d = \frac{\left|\overline{q_{CR}} - \overline{q_{IC}}\right|}{\sqrt{\frac{1}{2}\left(\sigma_{CR}^2 + \sigma_{IC}^2\right)}}$$

A high value of d indicated that the classifier was able to better discrimination between two conditions. For example, in our case, it means that the phases of theta or alpha oscillations coupled to the stimulus evoked HFA are clustered at different phase angles and separated with few overlaps. We tested the significance using a cluster-based permutation test and creating a distribution of pseudo discriminability indexes by randomizing the category labels (lure correct rejection versus lure false alarm) associated with high-frequency activity 100 times. Observed discriminability index above the 95th percentile of the surrogate data was considered significant.

Power-stratification controls—To ensure that the frequency specific pattern observed in the inter-regional phase synchrony (Figure 3A) and Granger causality effects (Figure 4A) were not due to the within-region conditional power differences, we repeated these analyses with power balanced across the relevant conditions (Figure S4). To select the power balancing trials across two conditions (lure correct rejection and lure false alarm), we performed a stratification method (ft_stratify.m from Fieldtrip Toolbox (Oostenveld et al., 2011)) to trim trials with extreme power values from each condition until the histogram of trial power values between two conditions were closely matched. We conducted this power-stratification control for both theta and alpha band power and selected the trials with balanced power for both frequency bands (n = 133 out of 663) to repeat the analysis of interregional phase synchrony and Granger causality.

Supplementary Material

Refer to Web version on PubMed Central for supplementary material.

ACKNOWLEDGMENTS

We thank I. Skelin, E.L. Johnson, R.F. Helfrich, A. Jafarpour, S.L. Leal, and L.D. Harriger for discussion; S.L. Leal for development of the task; H. Dong for help with preprocessing data; and the technicians and nurses of the UC Irvine Epilepsy Monitoring Unit. We are especially indebted to the patient volunteers at the UC Irvine Comprehensive Epilepsy Program. This work was supported by several grants from the NIH-NINDS R37NS21135 (to R.T.K.), NIMH R01MH102392 (to M.A.Y.), and NINDS T32NS45540 (to R.F.S.) (PI: T.Z. Baram)-as well as the UC Irvine School of Medicine Bridge Fund and the Ro- neet Carmell Memorial Endowment Fund support to J.J.L.

REFERENCES

Adolphs R, Tranel D, and Buchanan TW (2005). Amygdala damage impairs emotional memory for gist but not details of complex stimuli. Nat. Neurosci. 8, 512–518. [PubMed: 15735643]

Aftanas LI, Varlamov AA, Pavlov SV, Makhnev VP, and Reva NV (2002). Time-dependent cortical asymmetries induced by emotional arousal: EEG analysis of event-related synchronization and desynchronization in individually defined frequency bands. Int. J. Psychophysiol. 44, 67–82. [PubMed: 11852158]

Aghajan ZM, Schuette P, Fields TA, Tran ME, Siddiqui SM, Hasulak NR, Tcheng TK, Eliashiv D, Mankin EA, Stern J, et al. (2017). Theta Oscillations in the Human Medial Temporal Lobe during Real-World Ambulatory Movement. Curr. Biol. 27, 3743–3751. [PubMed: 29199073]

Amaral DG, and Cowan WM (1980). Subcortical afferents tothe hippocampal formation in the monkey. J. Comp. Neurol. 189, 573–591. [PubMed: 6769979]

Andersen P (2007). The hippocampus book (Oxford University Press).

Aru J, Aru J, Priesemann V, Wibral M, Lana L, Pipa G, Singer W, and Vicente R (2015). Untangling cross-frequency coupling in neuroscience. Curr. Opin. Neurobiol. 31, 51–61. [PubMed: 25212583]

Avants BB, Tustison NJ, Song G, Cook PA, Klein A, and Gee JC (2011). A reproducible evaluation of ANTs similarity metric performance in brain image registration. Neuroimage 54, 2033–2044. [PubMed: 20851191]

Axmacher N, Henseler MM, Jensen O, Weinreich I, Elger CE, and Fell J (2010). Cross-frequency coupling supports multi-item working memory in the human hippocampus. Proc. Natl. Acad. Sci. USA 107, 3228–3233. [PubMed: 20133762]

Bahramisharif A, Jensen O, Jacobs J, and Lisman J (2018). Serial representation of items during working memory maintenance at letter-selective cortical sites. PLoS Biol. 16, e2003805. [PubMed: 30110320]

Barnett L, and Seth AK (2014). The MVGC multivariate Granger causality toolbox: a new approach to Granger-causal inference. J. Neurosci. Methods 223,50–68. [PubMed: 24200508]

Bastos AM, Loonis R, Kornblith S, Lundqvist M, and Miller EK (2018). Laminar recordings in frontal cortex suggest distinct layers for maintenance and control of working memory. Proc. Natl. Acad. Sci. USA 115, 1117–1122. [PubMed: 29339471]

Bazelot M, Bocchio M, Kasugai Y, Fischer D, Dodson PD, Ferraguti F, and Capogna M (2015). Hippocampal Theta Input to the Amygdala Shapes Feedforward Inhibition to Gate Heterosynaptic Plasticity. Neuron 87, 1290–1303. [PubMed: 26402610]

Bohbot VD, Copara MS, Gotman J, and Ekstrom AD (2017). Low-fre-quencytheta oscillations in the human hippocampus during real-world and virtual navigation. Nat. Commun. 8, 14415. [PubMed: 28195129]

Bush D, Bisby JA, Bird CM, Gollwitzer S, Rodionov R, Diehl B, McEvoy AW, Walker MC, and Burgess N (2017). Human hippocampal theta power indicates movement onset and distance travelled. Proc. Natl. Acad. Sci. USA 114, 12297–12302. [PubMed: 29078334]

Buzsáki G, Anastassiou CA, and Koch C (2012). The origin ofextracellular fields and currents—EEG, ECoG, LFP and spikes. Nat. Rev. Neurosci. 13, 407–420. [PubMed: 22595786]

Cohen MX (2014). Analyzing neural time series data: theory and practice (MIT Press).

Cooper NR, Croft RJ, Dominey SJ, Burgess AP, and Gruzelier JH (2003).Paradox lost? Exploring the role of alpha oscillations during externally vs. internallydirected attention and the implicationsfor idling and inhibition hypotheses. Int. J. Psychophysiol. 47, 65–74. [PubMed: 12543447]

Delorme A, and Makeig S (2004). EEGLAB: an open source toolboxforanal-ysis of single-trial EEG dynamics including independent component analysis. J. Neurosci. Methods 134, 9–21. [PubMed: 15102499]

Ekstrom AD, Caplan JB, Ho E, Shattuck K, Fried I, and Kahana MJ (2005). Human hippocampal theta activity during virtual navigation. Hippocampus15, 881–889. [PubMed: 16114040]

Fries P (2005). A mechanism for cognitive dynamics: neuronal communication through neuronal coherence. Trends Cogn. Sci. 9, 474–480. [PubMed: 16150631]

Gordon JA (2016). On being a circuit psychiatrist. Nat. Neurosci. 19, 1385–1386. [PubMed: 27786177]

Grossman N, Bono D, Dedic N, Kodandaramaiah SB, Rudenko A, Suk HJ, Cassara AM, Neufeld E, Kuster N, Tsai LH, et al. (2017). Noninvasive Deep Brain Stimulation via Temporally Interfering Electric Fields. Cell 169, 1029–1041. [PubMed: 28575667]

Güntekin B, and Başar E (2014). A review of brain oscillations in perception of faces and emotional pictures. Neuropsychologia 58, 33–51. [PubMed: 24709570]

Haegens S, Nácher V, Luna R, Romo R, and Jensen O (2011). α-Oscillations in the monkey sensorimotor network influence discrimination performance by rhythmical inhibition of neuronal spiking. Proc. Natl. Acad. Sci. USA 108, 19377–19382. [PubMed: 22084106]

Hanslmayr S, Aslan A, Staudigl T, Klimesch W, Herrmann CS, and Bäuml KH (2007). Prestimulus oscillations predict visual perception performance between and within subjects. Neuroimage 37, 1465–1473. [PubMed: 17706433]

Hasselmo ME, and Stern CE (2014). Theta rhythm and the encoding and retrieval of space and time. Neuroimage 85, 656–666. [PubMed: 23774394]

Helfrich RF, and Knight RT (2016). Oscillatory Dynamics of Prefrontal Cognitive Control. Trends Cogn. Sci. 20, 916–930. [PubMed: 27743685]

Heusser AC, Poeppel D, Ezzyat Y, and Davachi L (2016). Episodic sequence memory is supported by a theta-gamma phase code. Nat. Neurosci. 19, 1374–1380. [PubMed: 27571010]

Huerta PT, and Lisman JE (1995). Bidirectional synaptic plasticity induced by a single burst during cholinergictheta oscillation in CA1 in vitro. Neuron 15, 1053–1063. [PubMed: 7576649]

Inman CS, Manns JR, Bijanki KR, Bass DI, Hamann S, Drane DL, Fasano RE, Kovach CK, Gross RE, and Willie JT (2018). Direct electrical stimulation of the amygdala enhances declarative memory in humans. Proc. Natl. Acad. Sci. USA 115, 98–103. [PubMed: 29255054]

Jacobs J, Hwang G, Curran T, and Kahana MJ (2006). EEG oscillations and recognition memory: theta correlates of memory retrieval and decision making. Neuroimage 32, 978–987. [PubMed: 16843012]

Jokisch D, and Jensen O (2007). Modulation of gamma and alpha activity during a working memory task engaging the dorsal or ventral stream. J. Neurosci. 27, 3244–3251. [PubMed: 17376984]

Jutras MJ, Fries P, and Buffalo EA (2013). Oscillatory activity in the monkey hippocampus during visual exploration and memory formation. Proc. Natl. Acad. Sci. USA 110, 13144–13149. [PubMed: 23878251]

Kensinger EA, and Schacter DL (2007). Remembering the specific visual details of presented objects: neuroimaging evidence for effects of emotion. Neuropsychologia 45, 2951–2962. [PubMed: 17631361]

Klimesch W, Sauseng P, and Hanslmayr S (2007). EEG alpha oscillations: the inhibition-timing hypothesis. Brain Res. Brain Res. Rev. 53, 63–88.

Kovach CK (2017). A Biased Look at Phase Locking: Brief Critical Review and Proposed Remedy. IEEE Trans. Signal Process 65, 4468–4480.

Lachaux JP, Rodriguez E, Martinerie J, and Varela FJ (1999). Measuring phase synchrony in brain signals. Hum. Brain Mapp. 8, 194–208. [PubMed: 10619414]

Lang PJ, Greenwald MK, Bradley MM, and Hamm AO (1993). Looking at pictures: affective, facial, visceral, and behavioral reactions. Psychophysiology 30, 261–273. [PubMed: 8497555]

Leal SL, and Yassa MA (2018). Integrating new findings and examining clinical applications of pattern separation. Nat. Neurosci. 21, 163–173. [PubMed: 29371654]

Leal SL, Tighe SK, Jones CK, and Yassa MA (2014a). Pattern separation of emotional information in hippocampal dentate and CA3. Hippocampus 24, 1146–1155. [PubMed: 24796287]

Leal SL, Tighe SK, and Yassa MA (2014b). Asymmetric effects of emotion on mnemonic interference. Neurobiol. Learn. Mem. 111, 41–48. [PubMed: 24607286]

Leal SL, Noche JA, Murray EA, and Yassa MA (2017). Age-related individual variability in memory performance is associated with amygdala-hippocampal circuit function and emotional pattern separation. Neurobiol. Aging 49, 9–19. [PubMed: 27723500]

Leutgeb JK, Leutgeb S, Moser MB, and Moser EI (2007). Pattern separation in the dentate gyrus and CA3 of the hippocampus. Science 315, 961–966. [PubMed: 17303747]

Lisman JE, and Jensen O (2013). The 0-y neural code. Neuron 77, 1002–1016. [PubMed: 23522038]

Loftus EF, Loftus GR, and Messo J (1987). Some Facts About Weapon Focus. Law Hum. Behav. 11, 55–62.

Lopour BA, Tavassoli A, Fried I, and Ringach DL (2013). Coding of information in the phase of local field potentials within human medial temporal lobe. Neuron 79, 594–606. [PubMed: 23932002]

Lundqvist M, Rose J, Herman P, Brincat SL, Buschman TJ, and Miller EK (2016). Gamma and Beta Bursts Underlie Working Memory. Neuron 90, 152–164. [PubMed: 26996084]

Marchewka A, Zurawski L, Jednorog K, and Grabowska A (2014). The Nencki Affective Picture System (NAPS): introduction to a novel, standardized, wide-range, high-quality, realistic picture database. Behav. Res. Methods 46, 596–610. [PubMed: 23996831]

McClelland JL, McNaughton BL, and O'Reilly RC (1995). Why there are complementary learning systems in the hippocampus and neocortex: insights from the successes and failures of connectionist models of learning and memory. Psychol. Rev. 102, 419–57. [PubMed: 7624455]

McGaugh JL (2013). Making lasting memories: remembering the significant. Proc. Natl. Acad. Sci. USA 110 (Supp/2), 10402–10407. [PubMed: 23754441]

Miller EK, Lundqvist M, and Bastos AM (2018). Working Memory 2.0. Neuron 100, 463–475. [PubMed: 30359609]

Min BK, and Herrmann CS (2007). Prestimulus EEG alpha activity reflects prestimulus top-down processing. Neurosci. Lett. 422, 131–135. [PubMed: 17611028]

Morrison SE, and Salzman CD (2010). Re-valuing the amygdala. Curr. Opin. Neurobiol. 20, 221–230. [PubMed: 20299204]

Nerad L, and Bilkey DK (2005). Ten-to 12-Hz EEG oscillation in the rat hippocampus and rhinal cortex that is modulated by environmental familiarity. J. Neurophysiol. 93, 1246–1254. [PubMed: 15738273]

Nolte G, Ziehe A, Nikulin VV, Schlögl A, Krämer N, Brismar T, and Muller KR (2008). Robustly estimating the flow direction of information in complex physical systems. Phys. Rev. Lett. 100, 234101. [PubMed: 18643502]

Oostenveld R, Fries P, Maris E, and Schoffelen JM (2011). FieldTrip: Open source software for advanced analysis of MEG, EEG, and invasive elec-trophysiological data. Comput. Intell. Neurosci. 2011, 156869. [PubMed: 21253357]

Orr G, Rao G, Houston FP, McNaughton BL, and Barnes CA (2001). Hippocampal synaptic plasticity is modulated by theta rhythm in the fascia dentata of adult and aged freely behaving rats. Hippocampus 11, 647–654. [PubMed: 11811658]

Parish G, Hanslmayr S, and Bowman H (2018). The Sync/deSync Model: How a Synchronized Hippocampus and a Desynchronized Neocortex Code Memories. J. Neurosci. 38, 3428–3440. [PubMed: 29487122]

Parvizi J, and Kastner S (2018). Promises and limitations of human intracranial electroencephalography. Nat. Neurosci. 21, 474–483. [PubMed: 29507407]

Peirce JW (2009). Generating Stimuli for Neuroscience Using PsychoPy. Front. Neuroinform. 2, 10. [PubMed: 19198666]

Pfurtscheller G (2001). Functional brain imaging based on ERD/ERS. Vision Res. 41, 1257–1260. [PubMed: 11322970]

Phelps EA (2004). Human emotion and memory: interactions of the amygdala and hippocampal complex. Curr. Opin. Neurobiol. 14, 198–202. [PubMed: 15082325]

Sauseng P, Klimesch W, Schabus M, and Doppelmayr M (2005). Frontoparietal EEG coherence in theta and upper alpha reflect central executive functions of working memory. Int. J. Psychophysiol. 57, 97–103. [PubMed: 15967528]

Seidenbecher T, Laxmi TR, Stork O, and Pape HC (2003). Amygdalar and hippocampal theta rhythm synchronization during fear memory retrieval. Science 301, 846–850. [PubMed: 12907806]

Staresina BP, Michelmann S, Bonnefond M, Jensen O, Axmacher N, and Fell J (2016). Hippocampal pattern completion is linked to gamma power increases and alpha power decreases during recollection. eLife 5, e17397. [PubMed: 27508355]

Stefanacci L, Suzuki WA, and Amaral DG (1996). Organization of connections between the amygdaloid complex and the perirhinal and parahippocam-pal cortices in macaque monkeys. J. Comp. Neurol. 375, 552–582. [PubMed: 8930786]

Stujenske JM, Likhtik E, Topiwala MA, and Gordon JA (2014). Fear and safety engage competing patterns of theta-gamma coupling in the basolateral amygdala. Neuron 83, 919–933. [PubMed: 25144877]

Talmi D, and Moscovitch M (2004). Can semantic relatedness explain the enhancement of memory for emotional words? Mem. Cognit. 32, 742–751.

Taylor JG, and Fragopanagos NF (2005). The interaction of attention and emotion. Neural Netw. 1S, 353–369.

Vinck M, Oostenveld R, van Wingerden M, Battaglia F, and Pennartz CM (2011). An improved index of phase-synchronization for electrophysio-logical data in the presence of volume-conduction, noise and sample-size bias. Neuroimage 55, 1548–1565. [PubMed: 21276857]

Wang X, Chen Y, and Ding M (2008). Estimating Granger causality after stimulus onset: a cautionary note. Neuroimage 41, 767–776. [PubMed: 18455441]

Watrous AJ, Deuker L, Fell J, and Axmacher N (2015). Phase-amplitude coupling supports phase coding in human ECoG. eLife 4, e07886.

Yassa MA, and Stark CE (2011). Pattern separation in the hippocampus. Trends Neurosci. 34, 515–525. [PubMed: 21788086]

Zheng J, and Lin JJ (2018). Modulating Amygdala-Hippocampal Network Communication: A Potential Therapy for Neuropsychiatric Disorders. Neuropsychopharmacology 43, 218–219. [PubMed: 29192669]

Zheng J, Anderson KL, Leal SL, Shestyuk A, Gulsen G, Mnatsakanyan L, Vadera S, Hsu FP, Yassa MA, Knight RT, and Lin JJ (2017). Amygdala-hippocampal dynamics during salient information processing. Nat. Commun. 8, 14413. [PubMed: 28176756]

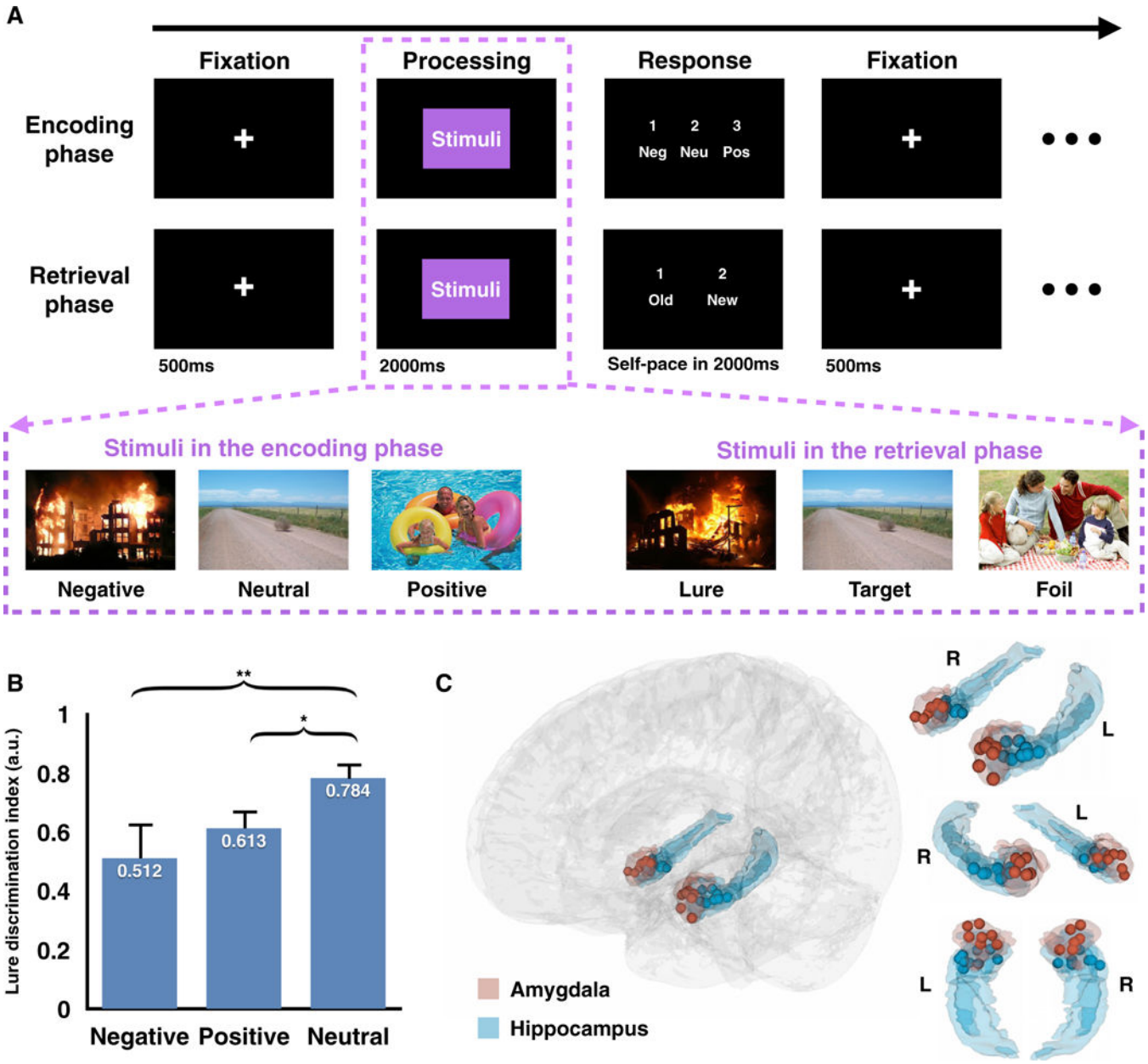

Figure 1. Experiment Design, Behavioral Results, and Electrode Locations

(A) Mnemonic discrimination task with emotional stimuli. Each trial consists of three parts: a 500-ms maintenance fixation period followed by a 2,000-ms image display (processing period) and a self-paced response window up to 2,000ms. During the encoding phase, participants were cued to rate the emotional valence of each stimulus (Neg, negative; Neu, neutral; Pos, positive). During the retrieval phase, participants were cued to identify the same stimuli presented in the encoding phase as old or to indicate similar scenes (lure items) and novel items(foil items) as new. See Table S4 and Figure S6 for visual controls of the stimuli set.

(B) Across all subjects, the lure discrimination index was significantly lower in negative and positive conditions compared to the neutral one (error bar, SEM; *$p < 0.05$, **$p < 0.01$,

Scheffé test). See Tables S1 and S2 for subjects' information and individual subject's behavior performance.

(C) Electrode localizations across 7 subjects, rendered onto athree-dimensional glass brain (gray) based on a high-resolution anatomical atlas, with amygdala electrodes in red and hippocampal electrodes in blue (L, left; R, right). See Figure S1 for individual electrode localization.

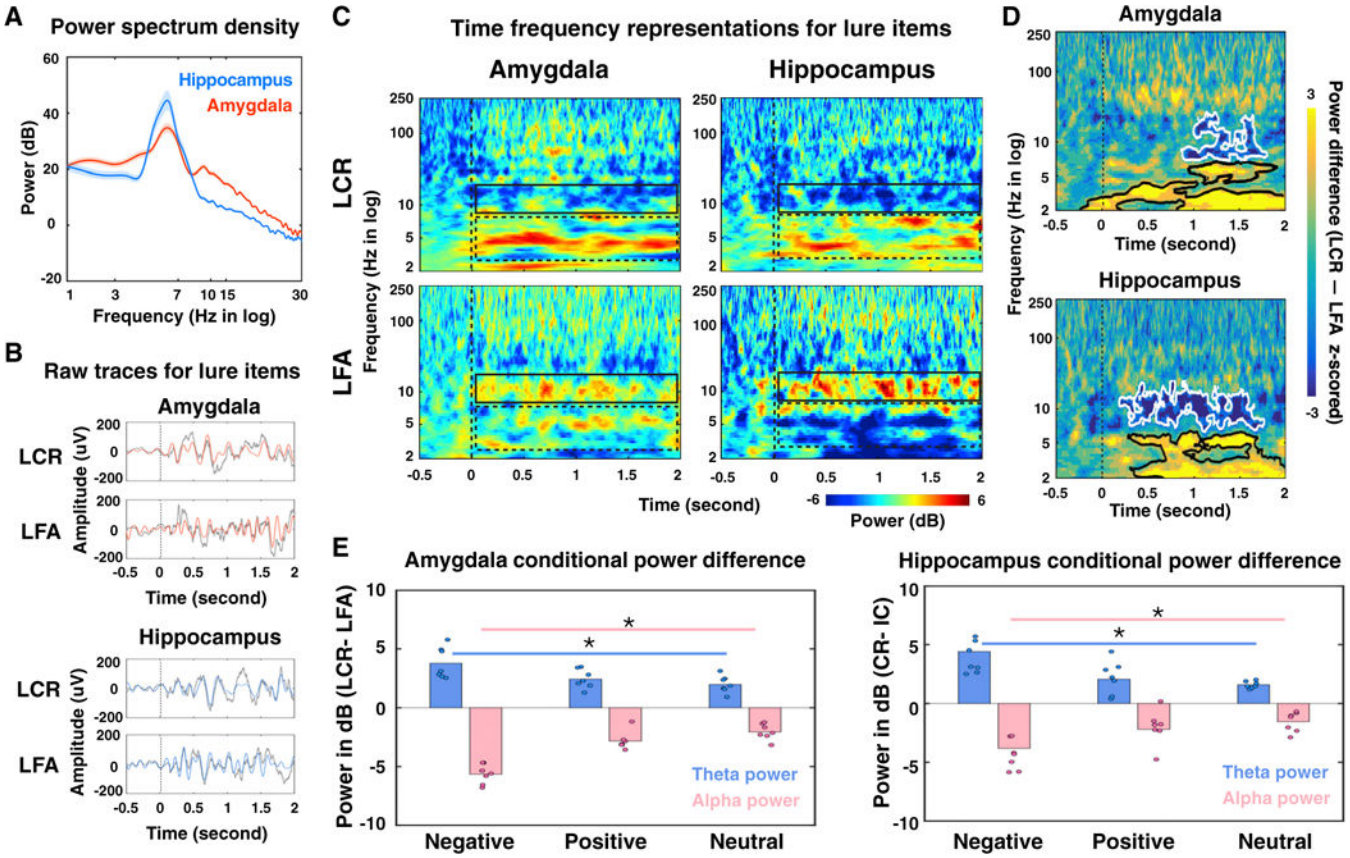

Figure 2. Task-Evoked Spectrotemporal Power in the Amygdala and the Hippocampus during Task Performances for Lure Items

(A) Averaged power spectra during the retrieval processing period in the amygdala (red) and the hippocampus (blue) for lure Items across all valence groups.

(B) Signal trial examples of local field potentials (LFPs) from a pair of electrodes in the amygdala (red) and the hippocampus (blue) from the same subject and the same LCR/LFA trial. Gray traces represent raw LFPs and red and blue lines denote LFPs filtered within 3–13 Hz. The vertical lines represent stimuli onsets. Slower oscillatory activity was observed during the LCR (~4 Hz) compared to the LFA (~7 Hz).

(C) Averaged power of electrodes in the amygdala (left) and the hippocampus (right) across all 7 subjects, normalized to the pre-trial baseline (500-ms fixation period) and grouped according to performance outcomes (LCR, top row; LFA, bottom row, collapsed across all valence groups). Warmer colors denote task-induced power increases from the baseline, while cooler colors refer to power decreases from the baseline. The relative power changes from the baseline within the theta and alpha bands are highlighted with dashed and solid boxes, respectively. Dashed vertical lines indicate stimuli onsets. See Figure S2 for the task-evoked spectrotemporal power for target hits and foil correct rejections and Table S3 for the comparisons of theta and alpha power between lure and target trials, as well as between lure and foil trials.

(D) Averaged power difference (LCR – LFA) across all 7 subjects and collapsed across all valence groups. Positive values (yellow colors) indicate greater power in the LCR compared to the LFA, while negative values (blue colors) refer to greater power in the LFA. The

significant conditional power differences ($p < 0.05$, corrected with the cluster-based permutation test) were highlighted with black contours (LCR > LFA) and white contours (LCR < LFA). Dashed vertical lines indicate the stimuli onset. Moreover, the power differences observed here were not driven by the influence of evoked response potentials (Figure S3).

(E) Conditional power difference (LCR – LFA) averaged within the significant theta (blue) and alpha (pink) clusters (detected in D) in the amygdala (left) and the hippocampus (right). Each dot represents the results of an individual subject. Power differences were plotted for negative, positive, and neutral valence stimuli (*$p < 0.05$).

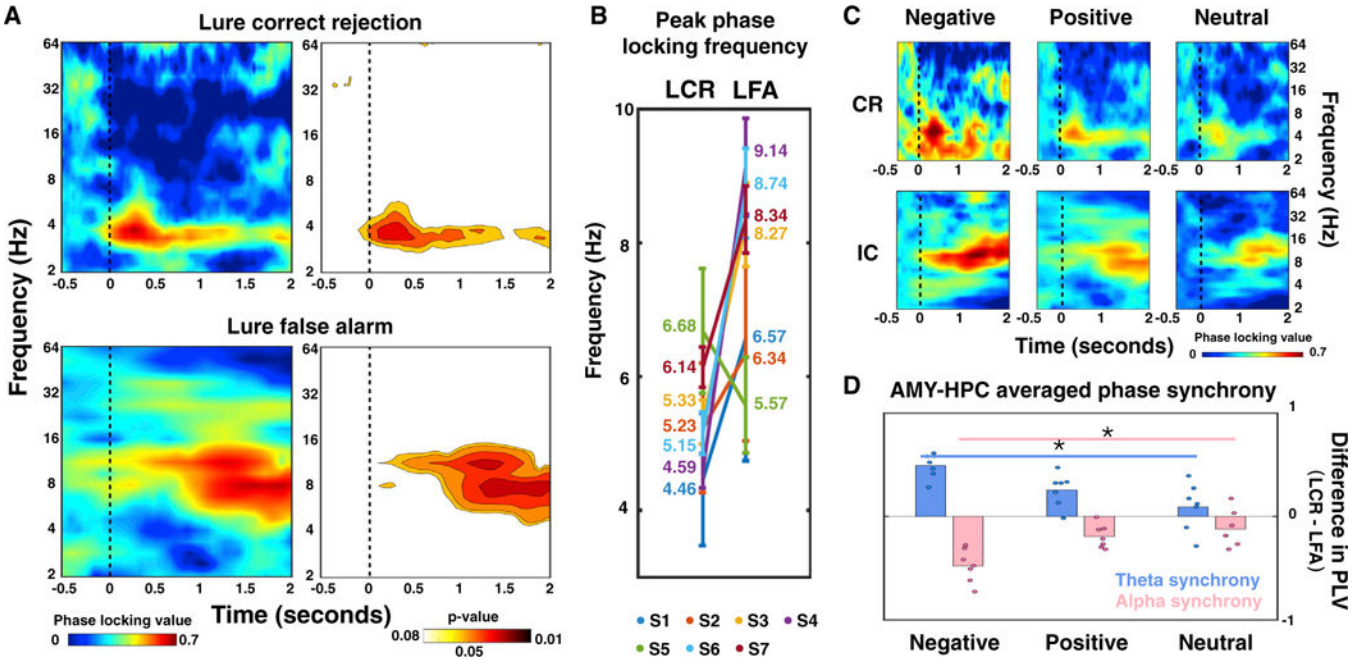

Figure 3. Frequency-Specific Amygdala-Hippocampal Phase Synchrony Reflects Discrimination Outcomes and Emotional Valence

(A) Amygdala-hippocampus synchrony (i.e., phase locking value [PLV]) averaged across all subjects, with stronger theta synchrony for LCRs(top left) and greater alpha synchrony for LFAs (bottom left). Phase locking value ranges from 0 to 1, with warmer colors indicating greater PLVs and stronger amygdala-hippocampal phase synchrony compared to baseline. The significant PLVs ($p < 0.05$, permutation test) were plotted for both conditions (right), with warmer colors denoting lower p values. The vertical dashed lines indicate stimuli onsets. The significant phase synchrony was not attributed to local power differences and was not due to volume conduction and uncorrelated noise (Figure S4).

(B) Peak frequency of amygdala-hippocampus synchrony for each subject (S1-S7, coded with different colors; the average peak frequency for each subject is labeled to the side in the plot), with theta synchrony for LCR and alpha synchrony for LFA.

(C) Consistent spectral patterns (theta synchrony for LCR and alpha synchrony for LFA) emerged with different emotional valence.

(D) Conditional differences in amygdala-hippocampus synchrony (LCR – LFA) are co-varied with emotional valence, with decreased theta synchrony (blue) and increased alpha synchrony (pink) for negative trials compared to neutral ones (*$p < 0.01$).

See Figure S5A and Table S3 for comparisons of theta and alpha phase synchrony between lure and foil trials.

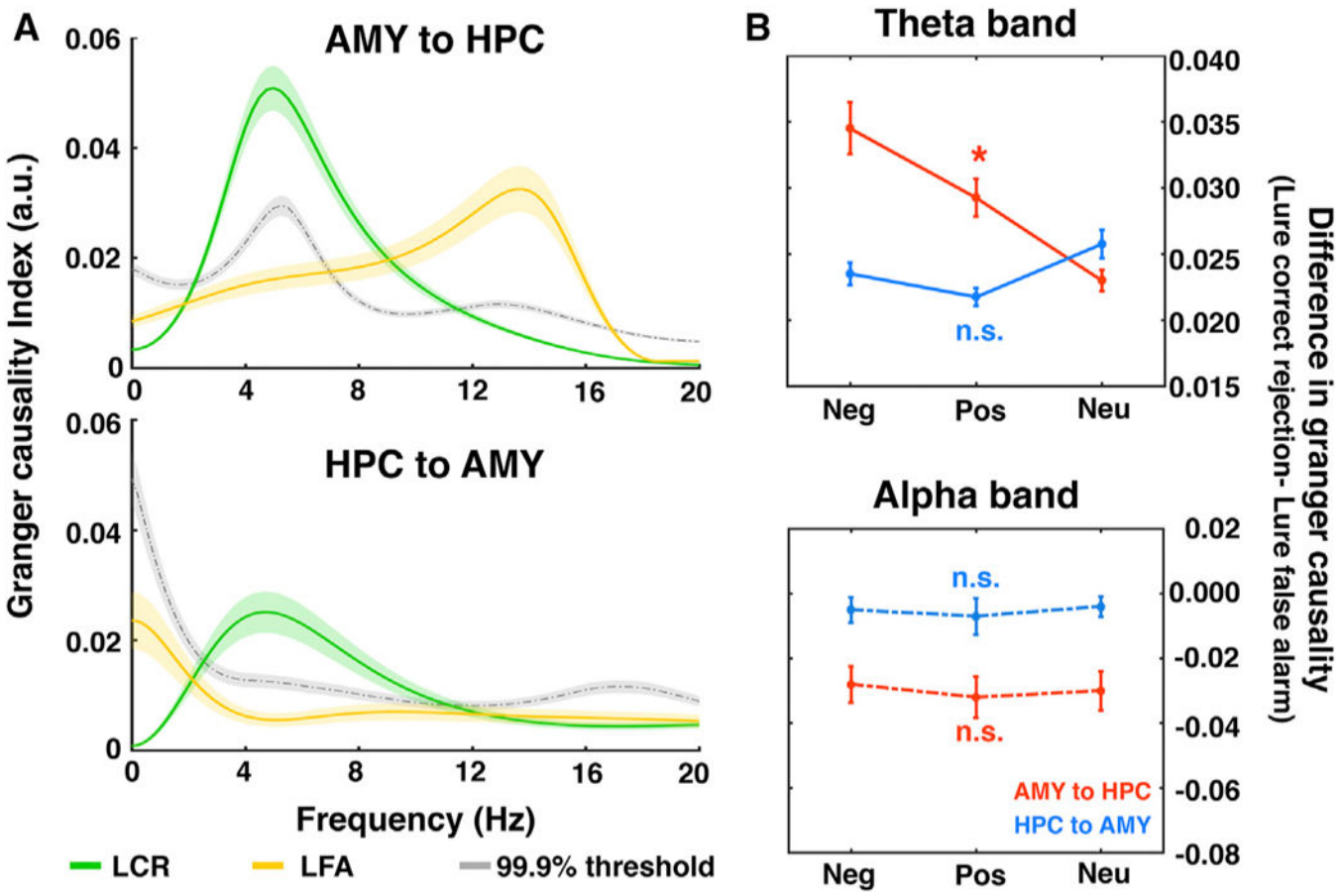

Figure 4. Bidirectional Amygdala-Hippocampal Interactions Support Mnemonic Discrimination

(A) Averaged Granger causality index across all subjects, with bidirectional interactions for LCRs (green lines) and unidirectional influence from the amygdala to the hippocampus for LFAs (yellow lines). The dashed gray lines represent the 99.9% threshold. Color shaded areas, SEM. The significant directional influence was not attributed to local power differences (Figure S4).

(B) Difference of Granger causality indices (LCR – LFA) averaged within the theta (top) and alpha (bottom) bands for both directions (red, amygdala to hippocampus; blue, hippocampus to amygdala). *$p < 0.05$ indicates that the conditional difference of Granger causality indices significantly differed across groups with different emotional valences.

Neg, negative; Pos, positive; Neu, neutral; n.s., not significant; AMY, amygdala; HPC, hippocampus. See Figure S5B for comparisons of directionality between lure and foil trials.

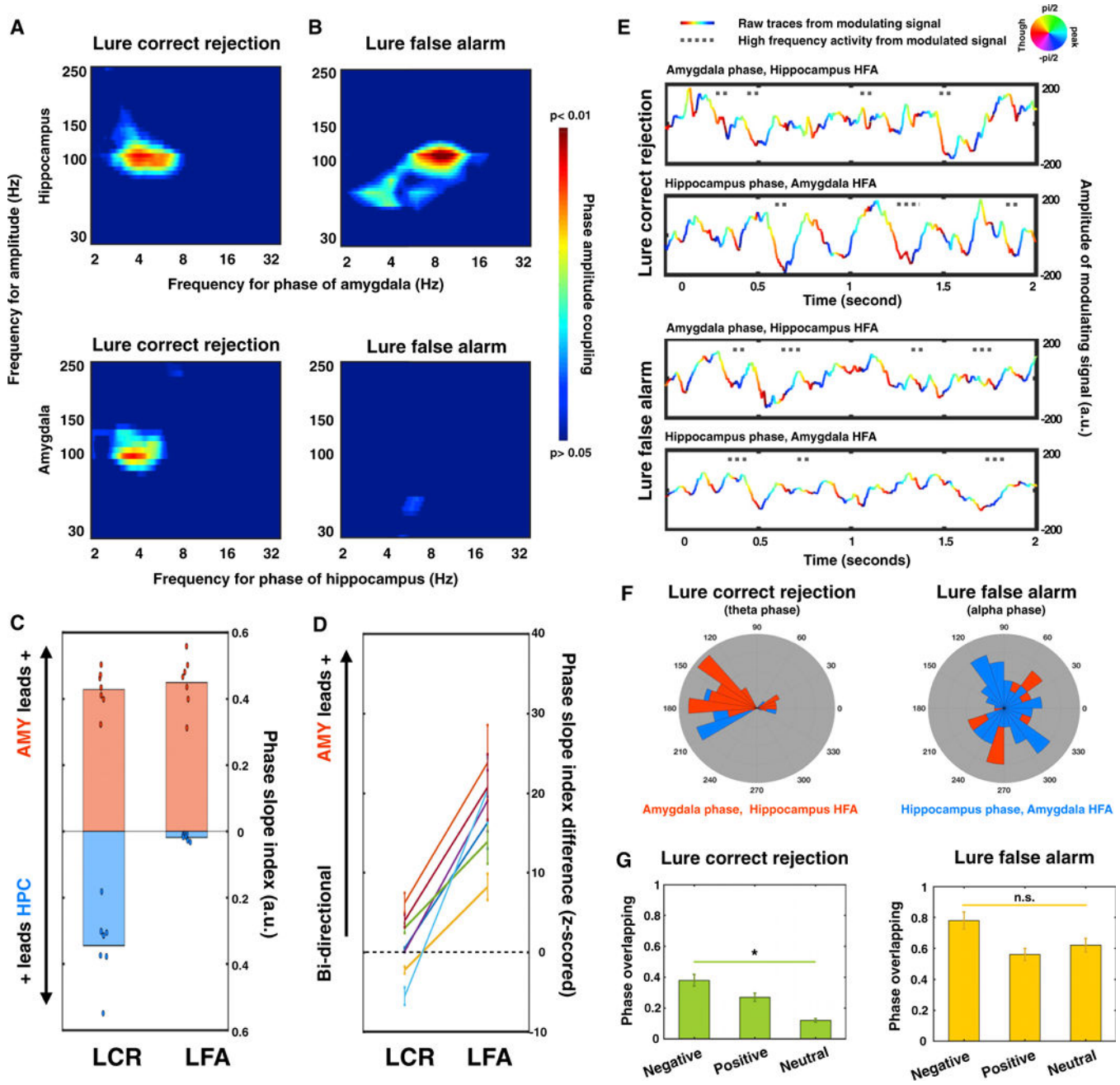

Figure 5. Distinct Theta Phases Encode Information from the Amygdala and the Hippocampus

(A) Averaged interregional phase-amplitude coupling (PAC) across all subjects within the amygdala-hippocampal network for LCRs (A) and LFAs (B). Warmer colors denote lower p values (permutation test; see STAR Methods).

(C) Phase slope indices (PSIs) were calculated for two directions (red, amygdala leads hippocampus; blue, hippocampus leads amygdala) in each condition (left, LCR; right, LFA). Positive values indicate low-frequency phases driving high-frequency activity. Dots represent the PSI value of each subject.

(D) PSI difference was calculated by subtracting the PSI values from two directions ($PSl_{AMYtoHPC} - PSl_{HPCtoAMy}$).Then, the calculated PSI differences were Z scored against null distributions generated by randomly shuffling trials. The colored lines represent the results of individual subjects. PSI differed between two conditions, from a bidirectional network during LCR to a unidirectional, amygdala-driven network during LFA ($p < 3.212 \times 10^{-12}$) (AMY, amygdala; HPC, hippocampus).

(E) Example trials from one subject demonstrate that high-frequency activity (HFA) occurred at different phases of theta oscillations for different conditions (LCR, top; LFA, bottom). The LFP traces were color coded by the phase of the peak modulating frequency from either the amygdala (top rows) or the hippocampus (bottom rows). Gray dots indicate the time when HFA from the modulated signal (top rows, hippocampus; bottom rows, amygdala) occurred.

(F) Circular distributions of phases at which HFA occurred across all 7 subjects.

(G) Overlapping percentage of the occurring phases of HFA from the amygdala and the hippocampus for both conditions (left, LCR; right, LFA). For LCR, the phase overlapping percentage reduced with the decrease of emotional valence (negative > positive > neutral, *$p < 0.05$). For LFA, the phase overlapping percentage remained constant across different emotional valence (n.s., not significant).

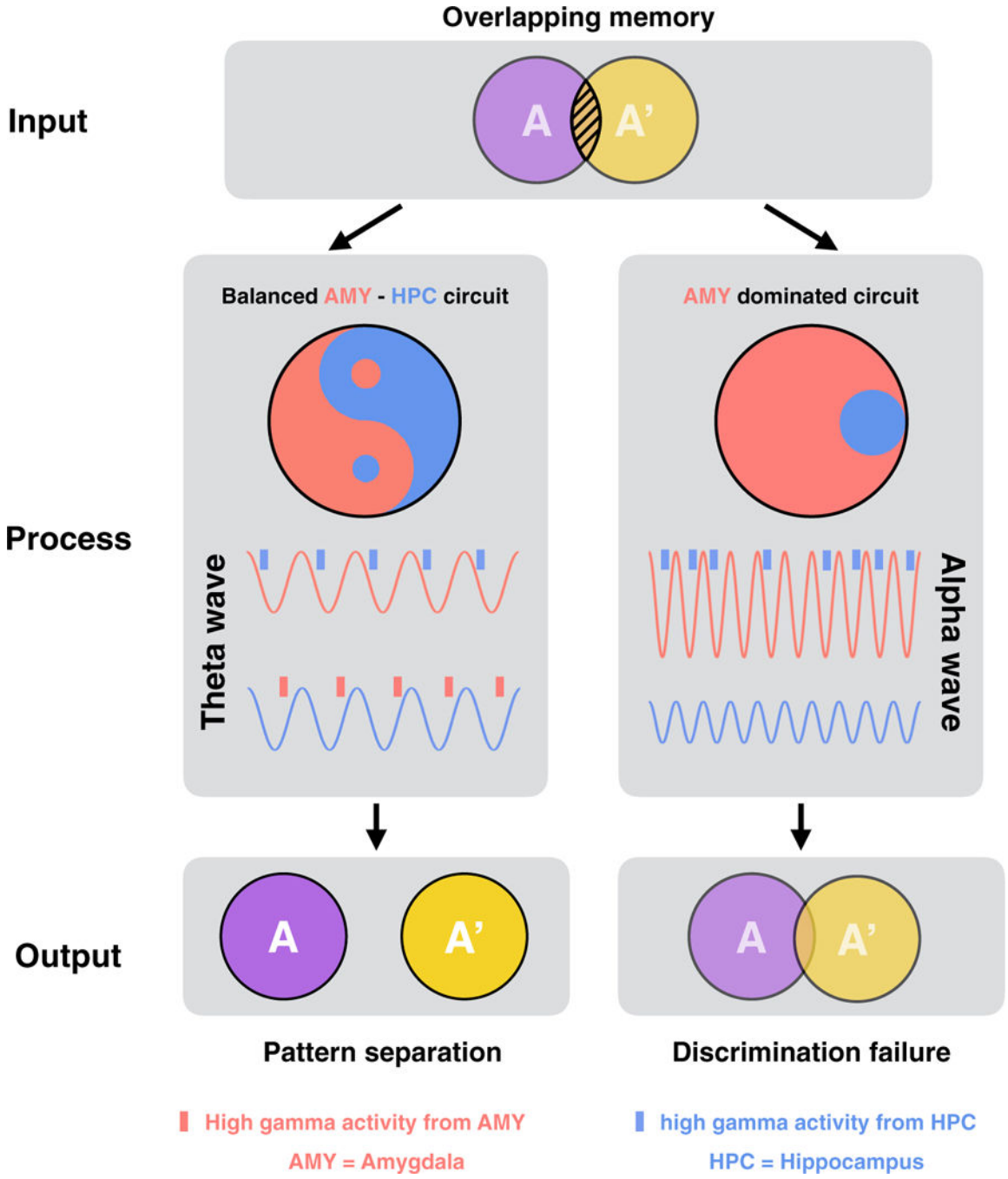

Figure 6. Interactive Approach between the Amygdala and the Hippocampus Determines Memory Outcomes

Differentiating similar (overlapping) memories from one another requires the cooperation between the amygdala and the hippocampus. A balanced amygdala-hippocampal circuit (left), with bidirectional interregional interactions via phase-specific theta-gamma coupling, could successfully separate the overlapping memories and store them as independent mnemonic representations (i.e., pattern separation). In contrast, an amygdala-dominated

circuit (right), with unidirectional influence from the amygdala to the hippocampus via alpha oscillations, could lead to discrimination errors.

KEY RESOURCES TABLE

REAGENT or RESOURCE	SOURCE	IDENTIFIER
Software and Algorithms		
Psychopy2	Peirce, 2009	https://www.psychopy.org/
MATLAB 2016b	MathWorks	RRID: SCR_001622
ANTs	Led by Brian Avants; Github	http://stnava.github.io/ANTs
The R project for Statistical Computing	Bell Laboratories	RRID: SCR_001905
EEGLAB 13_4_4b	Delorme and Makeig, 2004	http://sccn.ucsd.edu/eeglab/index.php
Multivariate Granger Causality (MVGC)	Barnett and Seth, 2014	https://users.sussex.ac.uk/~lionelb/MVGC/html/mvgchelp.html
FieldTrip 20170912	Oostenveld et al., 2011	http://www.fieldtriptoolbox.org/